Article

Comparative Study of Wind Energy Potential Estimation Methods for Wind Sites in Togo and Benin (West Sub-Saharan Africa)

Kwami Senam A. Sedzro [1][ID], Adekunlé Akim Salami [2,*], Pierre Akuété Agbessi [2] and Mawugno Koffi Kodjo [2]

[1] Transmission & Distribution Interactions, Grid Planning and Analysis Center, National Renewable Energy Laboratory, 15013 Denver West Pkwy, Golden, CO 80401, USA

[2] Department of Electrical Engineering, Ecole Nationale Supérieure d'Ingénieurs, Centre d'Excellence Régionale pour la Maîtrise de l'Electricité (CERME), University of Lomé, Lomé P.O. Box 1515, Togo

* Correspondence: asalami@univ-lome.tg; Tel.: +228-99469726

Abstract: The characterization of wind speed distribution and the optimal assessment of wind energy potential are critical factors in selecting a suitable site for wind power plants (WPP). The Weibull distribution law has been used extensively to analyze the wind characteristics of candidate WPP sites, and to estimate the available and deliverable energy. This paper presents a comparative study of five wind energy resource assessment methods as they applied to the context of wind sites in West Sub-Saharan Africa. We investigated three numerical approaches, namely, the adaptive neuro-fuzzy inference system (ANFIS), the multilayer perceptron method (MLP), and support vector regression (SVR), to derive the distribution law of wind speeds and to optimally quantify the corresponding wind energy potential. Next, we compared these three approaches to two well-known Weibull distribution law-based methods: the empirical method of Justus (EMJ) and the maximum likelihood method (MLM). Case study results indicated that the neural network-based methods, ANFIS and MLP, yielded the most accurate distribution fits and wind energy potential estimates, and consequently, are the most recommended methods for the wind sites in Togo and Benin. The orders of magnitude of the root mean squared error (RMSE) in estimating the recoverable energy using ANFIS were, respectively, 10-4 and 10-5 for Lomé and Cotonou, while MLP achieved an RMSE order of magnitude of 10-3 for both sites.

Keywords: wind energy potential; ANFIS; multilayer perceptron; support vector regression; probability density function; wind energy in Sub-Saharan Africa

1. Introduction

Energy is the essence of any country's development. For a long time, fossil energy sources have been driving the development of civilizations. In 2001, industrialized countries consumed more than half of the world's energy consumption [1]. Developing countries, in their industrial growth, would need to significantly increase their energy consumption. The increasing energy demand has been, for the most part, supplied by fossil fuels. Worldwide, fuel diversification and the increased adoption of renewable energy resources have garnered notable attention. Several renewable energy resources have been introduced in the energy portfolio of many countries around the world, with the most common ones being wind, geothermal, wave, tidal, and solar energy.

Even developing countries such as Benin and Togo, where industrialization is at an early age, have set their renewable energy targets. For reference, the average annual electrical energy consumption per capita in Benin and Togo is, respectively, 100 kWh [2] and 160 kWh [3], against 11,927 kWh [4] in the United States of America. However, on their paths to sustainable development, these countries have set national grid-connected renewable energy generation targets. The republic of Benin is targeting 44% by 2030, while

Togo is aiming for 30% by 2030 [5]. In addition, wind energy projects are expected to offset the energy deficit of these countries where access to electricity is still among the lowest in the world, with 29% [6] for Benin and 35% [7] for Togo. The technical potential for wind power is estimated at 322 MW for Benin and 73 MW for Togo [6,7]. We are interested in these countries, and more specifically in the sites of Lomé and Cotonou for their geographical positions and also for their ongoing wind power plant projects. This is the case of the Eco Delta project that will allow the construction of the first 25.2 MW wind power plant in Togo. With wind power capacity factors of 12.6 and 15.0%, Benin and Togo are decent candidates for wind power project development [5–7]. Benin and Togo are not the only countries interested in wind energy.

Recently, wind power generation has gained renewed interest worldwide, and is expected to actively contribute to reducing the emission of greenhouse gases [8–14]. However, despite the ecological advantage of wind power, the siting of wind power plants (WPP) is subject to detailed study in order to offer consumers competitive energy prices while ensuring a decent return on investment. It requires statistical analysis of the wind energy resource on the candidate sites in order to evaluate the feasibility and viability of the project [15]. Wind statistics are critical in determining the types of wind turbines to install. For an accurate estimate of return on investment, it is important to predict how much energy the WPP can generate over its lifetime. This paper reviews statistical analysis methods commonly used in wind energy resource assessment. The aim is to characterize the distribution law of wind speed measurements taken at the candidate WPP site with the objective of evaluating the wind energy potential. This study is important because wind speed is considered a random and intermittent variable; thus, a simple measurement is not enough to characterize the potential of a candidate WPP site [16]. Several distribution functions have been used in the literature to characterize distribution laws, such as the Gamma function [17–23], the inverse function of Gamma [22], the Rayleigh distribution, lognormal, normal, Pearson type V, kappa, Gumbel, binomial and the Weibull distribution function [24–33].

However, among the aforementioned functions, the Weibull distribution function is widely used to characterize wind speed distribution because it gives better results [34–36]. For instance, in [37], Elamouri and Amar Ben evaluated the wind potential at 17 sites in Tunisia using the meteorological method and the Weibull method; the Weibull distribution yielded more accurate results. Kiss and Jánosi [38] evaluated the surface wind speed covering a period of 44 years with a resolution of 6 h. They tested the well-known distribution functions, namely: Rayleigh, binormal, Weibull and lognormal. They observed that the Weibull function gave a better performance. They compared the Rayleigh, Weibull, lognormal, and binomial distribution functions and observed that the Weibull distribution function outperformed the three others. The Weibull distribution also proved effective in characterizing wind resources on the sea and parts of the land. A similar comparison was conducted in Turkey, and the distribution of Weibull prevailed over that of Rayleigh [39]. In Rwanda, Safari et al. showed, through a statistical investigation of wind characteristics and the evaluation of the wind potential, that the Weibull distribution outperformed that of Rayleigh [40]. The most commonly used Weibull distribution function is characterized by two parameters k and c and several numerical methods are available to determine these parameters [41–47]. Among them, the most well-known include the moment method (MM), the empirical method of Justus (EMJ), the maximum likelihood method (MLM) [48], the modified maximum likelihood method (MMLM), the energy pattern factor method (EPFM), the empirical method of Lysen (EML) and the graphic method (GM) [24,34,49,50].

In the search for a better approximation of the wind speed distribution law, other approaches were considered. Thiaw et al. used the multilayer perceptron (MLP) to evaluate the wind potential in Senegal and found that MLP gave a better result than the Weibull distribution, with 0.997 accuracy [16]. Carolin Mabel and E. Fernandez developed a neural network with three input parameters—wind speed, relative humidity, and generation times—and one output variable, the wind power plants' estimated energy output. This

model estimated the energy generated by seven wind power plants in India with a mean squared error of 0.0076 [51]. Celik and Kolhe set up a generalized feed-forward neural network (GFNN) to estimate the annual distribution of wind speed. The authors found that the GFNN produced a better wind speed distribution for calculating wind power generation for some wind turbines [52]. Mohandes et al. [53] used the adaptive neuro-fuzzy inference system (ANFIS) to estimate the wind speed profile and proved that ANFIS is a viable method for estimating wind speeds at high heights using low altitude velocity measurements. Asghar and Liu [49], in their recent work, used ANFIS to approximate the Weibull wind speed probability distribution function. The results obtained showed that this hybrid approach is more effective compared to numerical methods such as GM, EMJ, EML and EPFM.

In this paper, we aimed to estimate as accurately as possible the amount of wind energy that can be harnessed on the sites of Cotonou (Benin) and Lomé (Togo). In order to best fit the wind speed power density function of these sites, we surveyed five methods, namely the ANFIS, the MLP, the SVM, the EMJ and the MLM [23,54–56]. The main contributions of this paper are threefold:

- We first reviewed the most used methods for estimating wind energy potential and identified five that were promising based on their performance in existing literature;
- Next, we implemented and compared these five methods based on their performance when applied to the wind energy potential estimation problem in the context of two west African countries, Togo and Benin;
- Finally, we recommend the most accurate methods for future wind energy resource assessment projects in the region.

The remainder of the paper is organized as follows: Sections 2 and 3 focus on the five methods for wind energy potential evaluation investigated in this work. While Section 2 presents two Weibull-based methods, Section 3 describes three numerical methods. Section 4 discusses the details of the case study dedicated to the wind sites of Lomé (Togo) and Cotonou (Benin). The input data, method calibration and case study setup are presented in this section. Results from the case study are presented and discussed in Section 5. Section 6 concludes the paper.

2. Weibull Distribution-Based Methods for Wind Speed Characterization and Energy Potential Evaluation

Given that wind speed is a random variable, a simple measurement on a candidate site is insufficient for a sound estimation of its wind energy potential. Accurate prediction of continuous wind speed probability density is critical. The two-parameter Weibull distribution function is accepted and widely used in modeling wind speed distribution and in estimating the wind power density, which is important in assessing the energy potential of candidate wind sites and in evaluating the economic viability of WPP projects [49,57–60].

2.1. Wind Speed Characterization

The purpose of the Weibull-based wind speed characterization is to determine the Weibull parameters that best fit the Weibull distribution function to the histogram of site speed measurements.

The Weibull distribution function is characterized by three or two parameters [61,62]; the most used is the two-parameter one, given by (1)

$$f(v) = \frac{k}{c}\left(\frac{v}{c}\right)^{k-1}\exp\left[-\left(\frac{v}{c}\right)^{k}\right] \tag{1}$$

where $f(.)$ is the distribution law or the probability density, v the wind speed expressed in m/s, c the scale factor (same dimension as the speed), and k the form factor (dimensionless) characterizing the dissymmetry of the distribution.

When $k = 2$, the special Weibull distribution is known as Rayleigh distribution [63]. The cumulative function of the probability density function is given by (2) [64].

$$F(v) = 1 - exp\left[-\left(\frac{v}{c}\right)^k\right] \tag{2}$$

Various methods have been devised and used, in the literature, to estimate the parameters c and k of the Weibull function that would best fit a given empirical wind speed dataset. Among these methods we have the empirical method of Justus (EMJ) and the maximum likelihood method (MLM).

2.1.1. EMJ

Under the EMJ, the form factor k and the scale factor c are determined, respectively, by (3) and (4):

$$k = \left(\frac{\sigma}{\overline{v}}\right)^{-1086} \tag{3}$$

$$c = \frac{\overline{v}}{\Gamma\left(1 + \frac{1}{k}\right)} \tag{4}$$

where $\overline{v}$ and σ are the average and the standard deviation of the wind speed, and $\Gamma(.)$ the gamma function, generally known as the extension of the factorial function to complex numbers, given by (5) [65,66].

$$\Gamma(\alpha) = \int_0^\infty x^{\alpha-1} e^{-x} dx, \forall \alpha > 0 \tag{5}$$

2.1.2. MLM

Under the maximum likelihood method, the Weibull parameters k and c are obtained through numerical iterations [45,67]. The parameters k and c are estimated using (6) and (7) [68]. The form factor k is iteratively computed using (6) and replaced in (7) to determine the scale factor c.

$$k = \left[\left[\frac{\sum_{i=1}^n v_i^k ln(v_i)}{\sum_{i=1}^n v_i^k}\right] - \left[\frac{\sum_{i=1}^n ln(v_i)}{n}\right]\right]^{-1} \tag{6}$$

$$c = \left[\frac{\sum_{i=1}^n v_i^k}{n}\right]^{1/k} \tag{7}$$

In (6) and (7), v_i is the wind speed at time interval i, and n the number of non-zero wind speed data points.

2.2. Evaluation of the Wind Energy Potential

The notion of wind energy potential refers to the theoretical amount of wind energy available on a given site. The first step in estimating the energy potential of a wind site is the wind data collection. The intermittency and variability of wind makes it difficult to accurately predict its energy potential [16,69]. However, modeling the wind speed distribution helps to account for wind speed fluctuations and estimate the density of wind speed values not encountered during measurement. The wind speed distribution modelling consists of adjusting a known continuous distribution function (such as Weibull) to fit the histogram of the wind speed data collected on a candidate site. In case no distribution function is pre-assumed, numerical methods (such as ANFIS) are applied in order to learn and discover the distribution law hidden in discrete measurement data collected on the site. The wind energy potential is derived from the probability distribution of wind speed

according to Equations (8) through (10) [70]. The average wind power available P_m is given by (8):

$$P_m = \frac{1}{2}\rho \int_0^\infty f(v)v^3 dv \qquad (8)$$

where ρ is the air density, v the instantaneous wind speed, and $f(v)$ its probability density function.

The wind energy available E_a (in kWh/m^2) during a period of length T hours, is given by (9).

$$E_a = \frac{P_m}{1000}T \qquad (9)$$

The amount of energy that can be effectively recovered E_r on the site according to the characteristic power curve (see Figure 1) of the aerogenerator is given by (10):

$$E_r = \frac{T}{1000}\frac{1}{2}\rho S \left[\int_{V_s}^{V_r} f(v)v^3 dv + V_r^3 \int_{V_r}^{V_c} f(v)dv \right] \qquad (10)$$

where:

- $f(.)$: the probability distribution function;
- S: the area swept by the blades of the wind turbine;
- ρ: the air density;
- v: the instantaneous wind speed;
- V_s: the starting or cut-in speed of the wind turbine;
- V_r: the rated speed of the wind turbine;
- V_c: the maximum or cut-out speed of the wind turbine.
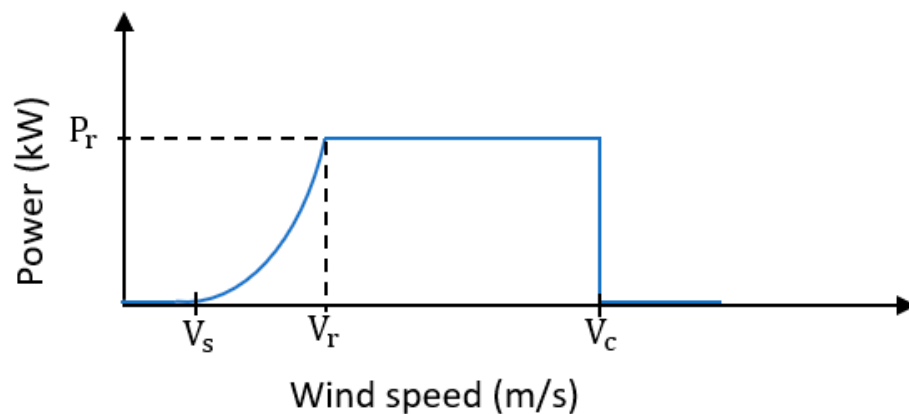

Figure 1. Power curve of a wind turbine.

Figure 1 shows the different operating regimes of a wind turbine.

The turbine output power varies as a function of the wind speed according to Equation (11).

$$P(v) = \begin{cases} 0 \; ; \; v < V_s \\ P_1(v) \; ; \; V_s < v < V_r \\ P_r \; ; \; V_r < v < V_c \\ 0 \; ; \; v > V_c \end{cases} \qquad (11)$$

The wind turbine power curve, showing the relationship between wind speed and output power, can be used to monitor and predict wind energy production [71].

In the interval $[V_s^k, V_r^k]$, the output power can be approximated as in (12)

$$P_1(v) = a_1 + b_1 v^k \qquad (12)$$

with the coefficients a_1 and b_1 defined by (13) and (14) obtained by solving (12) for the bounding speeds V_s and V_r:

$$a_1 = \frac{P_r V_s^k}{V_s^k - V_r^k} \tag{13}$$

$$b_1 = \frac{P_r}{V_s^k - V_r^k} \tag{14}$$

where k is the shape or form factor, the Weibull parameter defined above and P_r, the nominal or rated power.

The energy generated by the wind turbine E_g is then given by (15).

$$E_g = \frac{T}{1000} \int_{V_s}^{V_c} P(v) f(v) dv \tag{15}$$

3. Numerical Methods for Wind Speed Characterization

As well as the Weibull distribution-based methods presented in Section 3, we consider three numerical methods: the multilayer perceptron (MLP), the adaptive neuro-fuzzy inference system (ANFIS) and the support vector machine (SVM). The MLP method is based on neural networks, the ANFIS method combines the MLP and fuzzy logic, while the SVM method is based on the concept of maximum margin and kernel. These methods are widely used in figure recognition, prediction, classification, and regression analysis [72]. They offer an alternative way of dealing with complex and ill-defined problems [73]. In the context of energy potential estimation, these numerical methods take as input discrete measured wind speed values (Vi) and adjust their intrinsic parameters in a way that minimizes the discrepancy between the model output (fi) and the actual speed frequencies (Fi). Once model parameters are set through this learning process, continuous distribution laws $f(.)$ are derived as the model output of a continuous range of wind speed values v.

3.1. The Multilayer Perceptron Approach

An artificial neural network (ANN) can be defined as a complex network consisting of interconnected networks formed by elementary computing units or nodes called neurons. Neurons are organized in layers and can be connected in different ways. The topology of the connection between neurons, which depends on the problem to be solved, defines the architecture of the network. ANNs are "trained" to perform tasks by considering examples made of a set of input values and a set of corresponding output values [16]. The network must "learn" in order to be able to provide correct answers for other unknown entries. The training stage helps evaluate and meet performance criteria which is to minimize the error between the network output and the actual training output values. In the case of wind speed distribution law prediction, examples are made of discrete wind speed measurements (Vi) and their corresponding inferred frequencies (Fi).

Different types of ANNs exist. The MLP-type ANNs are the most widely used, especially in nonlinear regression problems [74,75]. An MLP ANN includes one or more hidden layers activated by sigmoid functions and one output layer. Figure 2 illustrates a two-input MLP network comprising a hidden layer with three neurons and a one-neuron output layer. The neurons of the hidden layer L receive information from the neurons of layer L − 1 and are connected to the neurons of layer L + 1. Neurons of the same layer do not share any connection. Each neuron in the output layer performs a non-linear function of the input layer. More information on the MLP can be found in [75–77]. The potential s_i of a neuron i and its activation O_i are given, respectively, by the Equations (16) and (17).

$$s_i = \sum_{j=1}^{p} w_{ij} x_j + b_i \tag{16}$$

where p denotes the number of neurons of the upstream layer connected to neuron i; x_j represents the j-th input of neuron i; w_{ij} (or interchangeably w_{ji}) is the weight of the connection between neuron i and neuron j (of the upstream layer); b_i is the bias; $h_i(.)$ the activation function of the neuron i.
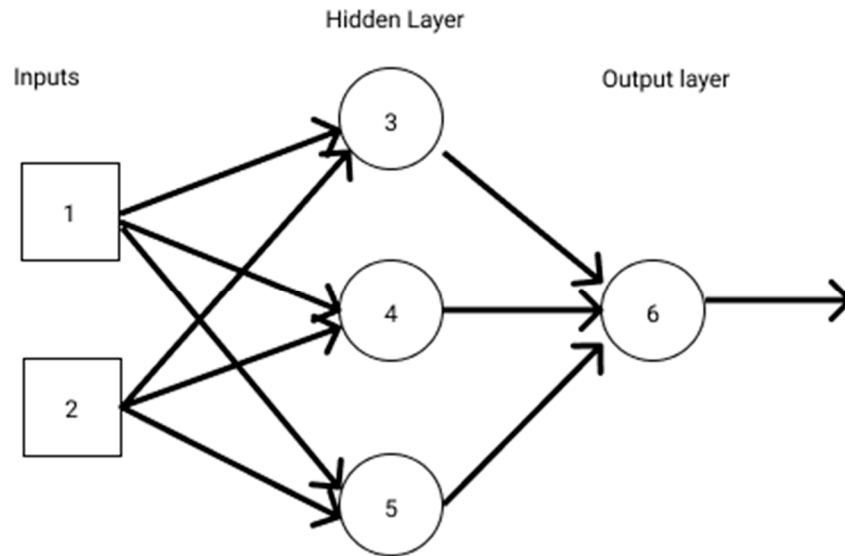

Figure 2. The architecture of a multilayer perceptron.

For the purposes of wind speed characterization and energy potential estimation, the designed MLP ANN will receive wind speed data as input and produce wind speed frequencies as output, which will be used to fit the actual wind speed histogram.

3.2. ANFIS

The adaptive neuro-fuzzy inference system (ANFIS) can be described as a fuzzy model of Sugeno in the framework of an adaptive system to facilitate learning and adaptation. What makes ANFIS a powerful approach is that it takes advantage of the learning ability of neural networks and human reasoning. Figure 3 shows the basic architecture of ANFIS.

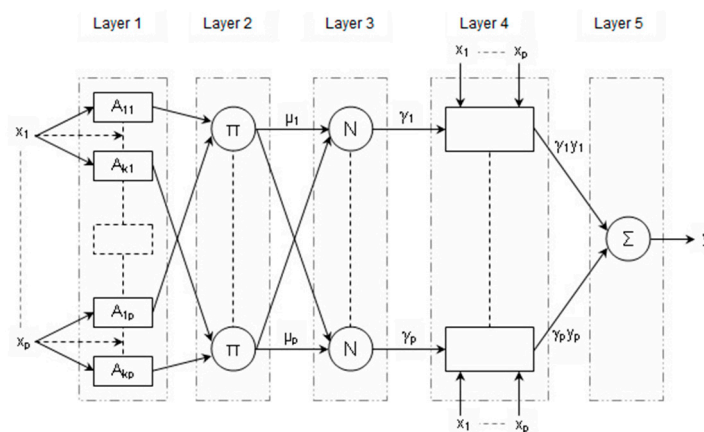**Figure 3.** The architecture of ANFIS.

Architecturally, the ANFIS is structured in five layers. In the fuzzification layer (layer 1), membership functions are assigned to each input variable. There are as many neurons as membership functions assigned to the input variables. The weight assigned to each neuron is updated during the learning process. Trapezoidal, sigmoid, triangular, and Gaussian

functions are the most commonly used membership functions. The Gaussian membership function which can be tuned by the mean c and the standard deviation σ is given by (18):

$$\mu(x)_i = e^{-\frac{1}{2}\left[\frac{(x-c_i)^2}{\sigma_i^2}\right]}$$

(17)

where i is index of membership function; c_i and σ_i characterize the center and breadth of the i-th Gaussian membership function.

Layer 2 computes the product of all incoming signals from the fuzzification layer as presented in (19). The resulting output of this layer represents the firing strength of each fuzzy rule. There are as many fuzzy rules as nodes in layer 2.

$$w_i = \mu(x)_i * \mu(x)_{i+1}$$

(18)

Layer 3 is the normalization layer in which each node normalizes the membership degree of a given fuzzy rule. The output represents the participation of each fuzzy rule in the result [78] and presented by (20).

$$\overline{w_i} = \frac{w_i}{\sum w_i}$$

(19)

Layer 4 is an adaptive layer resulting in the product of each Takagi–Sugeno linear function representing the conclusion of an inference rule with its normalized participation factor obtained by layer 3. The output is given by (21) where p_i and r_i are known as consequence parameters.

$$\overline{w_i}.y_i = \overline{w_i}(p_i x + r_i)$$

(20)

Layer 5 sums all outputs from the defuzzification nodes as shown by (22).

$$y = \sum \overline{w_i}.y_i = \frac{\sum w_i.y_i}{\sum w_i}$$

(21)

The input and output in the ANFIS approach are the same as in MLP presented in session 3.1.

3.3. SVR

Support vector machines (SVMs) have gained immense popularity in fields such as computer science, hydrology and environmental research [34]. However, their application is mainly in the recognition of figures, prediction, classification and in regression analysis [72]. Generally, SVMs perform better than other traditional techniques such as neural networks and other conventional statistical models [79,80].

The variant of the SVM considered in this study is the support vector regression (SVR). Depending on the type of problem at hand, one might choose between linear SVR and nonlinear SVR. The purpose of SVR is to approximate a set of data (x_i, y_i) by a function $f_{w,b}$ defined by (23) in the linear case such that (24) is satisfied.

$$f_{w,b}(x) = \langle w, x \rangle + b$$

(22)

$$\left| f_{w,b}(x_i) - y_i \right| \leq \varepsilon, \forall i \in [1, n]$$

(23)

The idea is to minimize the term w while making sure not to exceed a predefined error rate ε. From a graphical point of view, this amounts to finding a zone of the plane, of width

2ε called the tube, that contains all examples x_i. Considering the minimization of $\|w^2\|$, we obtain the quadratic problem given by (25):

$$\min\left\{\frac{1}{2}\|w\|^2\right\}$$
$$subject\ to\ :\ \begin{cases} y_i - \langle w, x_i \rangle - b \leq \varepsilon \\ \langle w, x_i \rangle + b - y_i \leq \varepsilon \end{cases} \tag{24}$$

This formulation of the problem considers that there exists a linear function $f_{w,b}(x) = \langle w, x \rangle + b$ that approximates all the examples with a precision ε. This assumption is not always true in practice. In the presence of outliers, it is important to allow for flexible error margins. In this case, the concept of a flexible margin is used. It consists of introducing slack variables ζ_i, ζ_i^* to ensure the existence of feasible solutions. The optimization problem in (25) becomes the one given by (26):

$$\min\left\{\frac{1}{2}\|w\|^2\right\}$$
$$subject\ to\ :\ \begin{cases} y_i - \langle w, x_i \rangle - b \leq \varepsilon \\ \langle w, x_i \rangle + b - y_i \leq \varepsilon \end{cases} \tag{25}$$

$$min\left\{\frac{1}{2}\|w\|^2 + C\sum_{i=1}^{n}(\zeta_i + \zeta_i^*)\right\}$$
$$subject\ to\ :\ \begin{cases} y_i - \langle w, x_i \rangle - b \leq \varepsilon + \zeta_i \\ \langle w, x_i \rangle + b - y_i \leq \varepsilon + \zeta_i^* \end{cases} \tag{26}$$

The constant C ($C > 0$), a penalty factor, is a hyper parameter allowing the tradeoff between flexibility and cost to be adjusted. This formulation is equivalent to using an *ε-insensitive* error function $|\zeta|_\varepsilon$ defined by (27).

$$|\zeta|_\varepsilon = \begin{cases} 0,\ if\ |y - f_{w,b}(x)| \leq \varepsilon \\ |y - f_{w,b}(x)| - \varepsilon,\ if\ |y - f_{w,b}(x)| \succ \varepsilon \end{cases} \tag{27}$$

This function can be interpreted as creating an insensitivity tube of radius ε around the function $f_{w,b}(x)$. $|\zeta|_\varepsilon$ represents the distance along the y-axis between the point (x_i, y_i) and the edge of the tube. From the dual formulation and the Lagrange equation, the objective function obtained can be written in the form of (28):

$$f(x) = \sum_{i=1}^{n}(\alpha_i + \alpha_i^*)\langle x_i, x \rangle + b \tag{28}$$

where α_i and α_i^* are the Lagrange multipliers derived from the dual formulation.

As data becomes more complex, non-linear regression problems are solved using kernel functions. The data is projected from the input space into a larger dimension space. The generalized form of the cost function given by (29):

$$f(x) = \sum_{i=1}^{n}(\alpha_i + \alpha_i^*)K(x_i, x) + b \tag{29}$$

where $K(.)$ is a kernel function.

Table 1 shows the most common kernels used in solving non-linear problems.

Table 1. Types of kernels.

Kernel	Mathematical Expression	
Linear	$K(x,y) = \langle x, y \rangle$	(30)
Polynomial	$K(x,y) = (a\langle x, y \rangle + b)^d$	(31)
Gaussian	$K(x,y) = \exp\left(-\frac{\|x-y\|^2}{2\sigma^2}\right)$	(32)

As mentioned in Section 2, the output of the three numerical methods (MLP, ANFIS and SVR) presented in Section 3 is a prediction of the distribution function of the wind speed on candidate wind power plant sites. Next, the energy potential is obtained using Equation (15).

4. Case Study

The aim of this work being a comparative evaluation of the wind energy potential in Benin and Togo, we applied the distribution estimation techniques presented in Sections 2 and 3 to these two West African countries. Benin and Togo enjoy a tropical climate. With an average annual rainfall of 1244 mm in Cotonou and 859 mm in Lomé, both sites experience an average annual temperature of 26.8 °C (80.24 °F) and share two seasons: one dry—the harmattan, and one rainy—the monsoon.

4.1. Data

The wind data used in this study for the site of Cotonou was collected at the International Airport of Cotonou (COO) at 6.35° N and 2.38° E, and at an altitude of 9 m. As for the site of Lomé, the wind data was collected at Gnassingbé Eyadema International Airport (LFW) at a latitude of 6.17° N, a longitude of 1.25° E and an altitude of 25 m. The windiest month on both sites is September with an average wind speed of 5.0599 m/s (11,185 mi/h) in Cotonou and 4.6832 m/s (8.948 mi/h) in Lomé. The wind speed data spanned the period from January 2003 through December 2015 for a total of 13 years.

Given that the wind speed measurements were not taken at the altitude where wind turbines will be deployed, there was a need to extrapolate the wind speed values to the turbine hub height by means of the power law model of the vertical wind profile proposed by Hellman [81] and expressed in Equation (33) [82–84].

$$\frac{v}{v_0} = \left(\frac{h}{h_0}\right)^{\alpha} \tag{33}$$

where v is the extrapolated wind speed at altitude h, given the measured speed v_0 at altitude h_0. The wind shear coefficient also known as Hellman (or friction) coefficient α typically ranges from 0.40 in areas with tall buildings to 0.10 over smooth, hard ground, lakes or ocean [85–92]. For Lomé and Cotonou, because the measurements were taken in airport areas, we chose $\alpha = 0.1$ in this study.

Figure 4 shows the wind speed histograms of the sites of Lomé and Cotonou, for wind speed values adjusted to 10 m altitude.
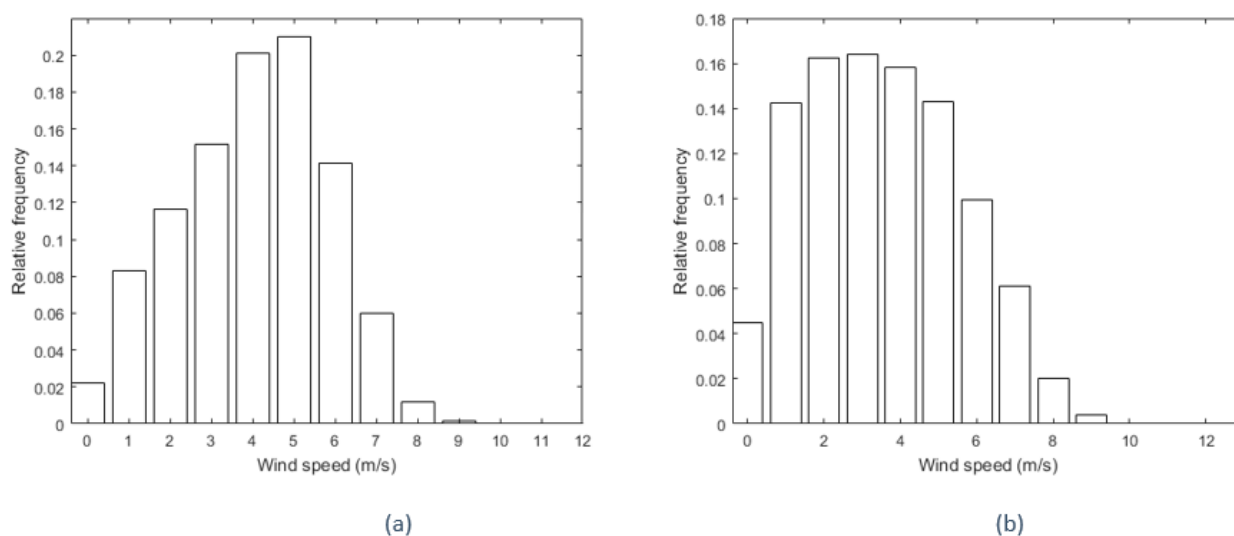

(a)

(b)

Figure 4. Wind speed distribution on the sites of Cotonou (**a**) and Lomé (**b**) at 10 m high.

4.2. Wind Turbine

Three candidate wind turbines (E-44, E-48, E-53) were considered based on existing work by Mudasser et al., and Salami et al. as well as on ENERCON reviews [93–98]. The characteristics of these wind turbines are given in Table 2.

Table 2. Characteristics of wind turbines.

Title 1	E-44	E-48	E-53
Cut-in speed (m/s)	3	3	3
Rated speed (m/s)	16	12	12
Cut-out speed (m/s)	25	25	25
Rated output power (kW)	900	800	800
Blade diameter (m)	44	48	52.9
Hub	60	76	73

Normally the cut-off speed will vary between 28 and 34 m/s. However, in our study, a speed of 25 m/s was assumed due to the absence of the power curve beyond this speed. Figures 5–7 show the modelling of the power curve of these wind turbines by the numerical methods used in the document.
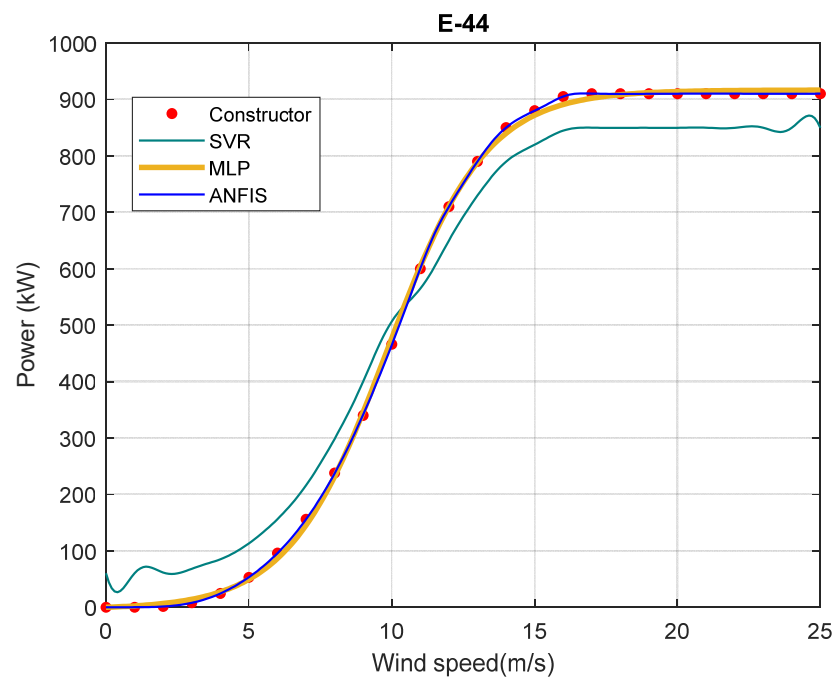
Figure 5. Characteristic power curve modeling for E-44.

To make the optimal choice of the wind turbine to be used, the average energy produced on the sites was calculated. The results are shown in Table 3.

Table 3. Average annual energy output at different hub heights.

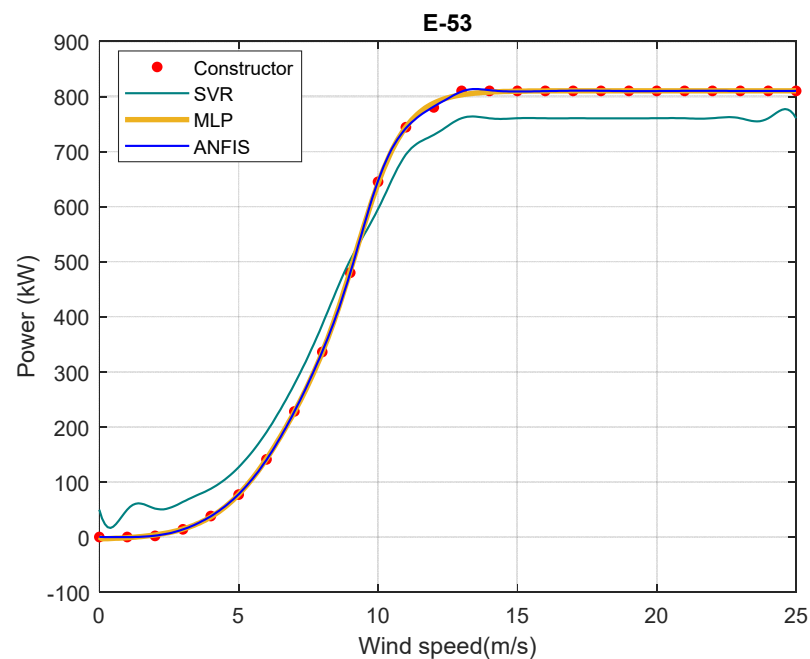| Hub Height (m)	Wind Turbine	Lomé	Cotonou
60	E-4	49,688.15	56,828.55
76	E-48	65,667.14	74,709.54
73	E-53	77,535.48	88,284.59

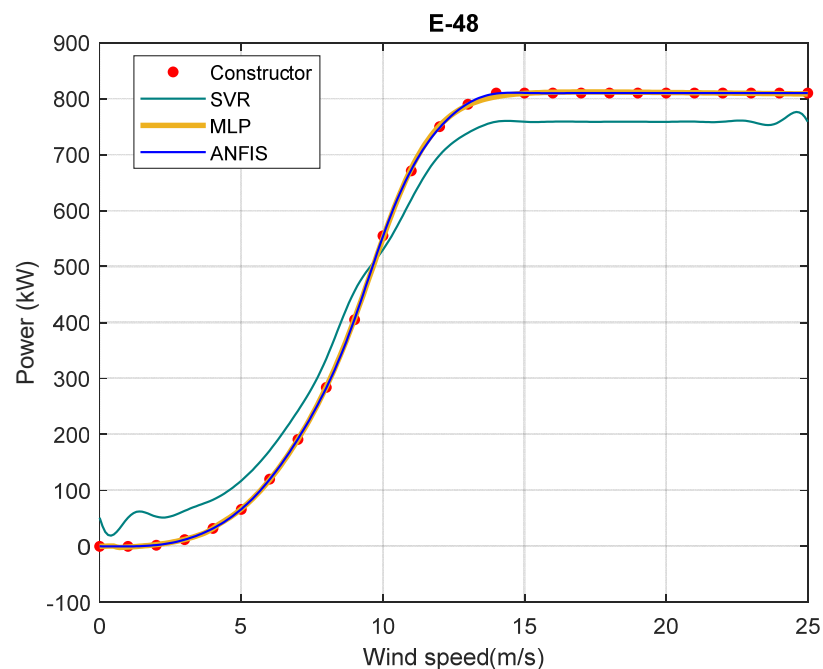**Figure 6.** Characteristic power curve modeling for E-48.

Figure 7. Characteristic power curve modeling for E-53.

It was found that the E-53 wind turbine produces an average energy of 77.54 MW at an altitude of 73 m which is relatively high, then follows the E-48 with an average energy of 65.67 MW at a height of 76 m and the E-44 finishes the list at 49.69 MW, with a height of 60 m. With a rated power of 800 kW and a rated speed of 13 m/s and a mast height of 73 m, the E-53 wind turbine was chosen as the most cost-effective wind turbine on both sites.

4.3. Metrics for Performance Evaluation

We evaluated the performance of the aforementioned methods using two indices that account for the magnitude of error margins. The lower the error margin, the more accurate the method. In this work, we used the root mean square error (RMSE) and the coefficient of determination (R^2) or R-squared.

4.3.1. RMSE

The root mean squared-error (RMSE) compares estimated data against measured data according to the formula of relation (34) [45,99]:

$$\text{RMSE} = \sqrt{\frac{1}{n}\sum_{i=1}^{n}(X_{i,est} - X_{i,act})^2} \tag{34}$$

where $X_{i,est}$ is the estimated value and $X_{i,act}$, the actual value. It is always positive and does not capture the dominant direction of deviation.

4.3.2. R^2

R^2 provides the linear relationship between the estimated data and the actual or measured data, as given by (35).

$$R^2 = \frac{\sum_{i=1}^{n}(X_{i,act} - X_{act,moy})^2 - \sum_{i=1}^{n}(X_{i,est} - X_{i,act})^2}{\sum_{i=1}^{n}(X_{i,act} - X_{act,moy})^2} \tag{35}$$

where $X_{act,moy}$ is the average value of the measured or observed data, and $X_{i,est}$, the estimated value.

4.4. Method Calibration

In this section, we discuss how the Weibull, MLP, SVR, and ANFIS methods were calibrated in our case study. Specifically, we present the parameter selection process for the sites of Cotonou and Lomé.

4.4.1. Weibull Parameters from Distribution-Based Methods

The Weibull distribution-based methods considered in this study are the empirical method of Justus (EMJ) and the maximum likelihood method (MLM). The Weibull parameters k and c used for each of these methods were computed based on the formulas presented in Section 2.1. Table 4 shows these parameters for the sites of Cotonou and Lomé.

Table 4. Weibull parameters obtained with EMJ and MLM for the sites of Cotonou and Lomé.

Methods	Lomé		Cotonou	
	k	c	k	c
EMJ	1.8233	3.9704	2.3671	4.5264
MLM	2.0310	4.1788	2.5722	4.6173

4.4.2. MLP Design

The multilayer perceptron neural network considered in this study is a single-input single-output network (see Figure 2). The input receives wind speed series and the output produces the probability densities. The output layer has a single neuron. We explored 7 designs of the hidden layer with the number of neurons ranging from 4 to 10 as shown in Table 5. Based on the error values (RMSE), the number of neurons in the hidden layer was fixed at 9 where the lowest RMSE values were reached for both Cotonou and Lomé.

Table 5. Choice of the number of neurons.

Number of Neurons in the Hidden Layer	RMSE	
	Lomé	Cotonou
4	1.84×10^{-3}	5.34×10^{-3}
5	1.68×10^{-3}	4.88×10^{-3}
6	3.88×10^{-4}	4.87×10^{-3}
7	4.15×10^{-4}	1.27×10^{-3}
8	4.16×10^{-4}	1.45×10^{-5}
9	8.02×10^{-5}	1.78×10^{-5}
10	9.56×10^{-4}	1.98×10^{-5}

4.4.3. ANFIS Design

The type and number of membership functions are two critical parameters in the design of any adaptive neuro-fuzzy inference system. Tables 6 and 7 present the performance of a set of combinations of both parameters. On the nature of the membership functions, we evaluated four membership functions, namely, the Gaussian function, the sigmoidal function, the triangular function and the trapezoidal function. Because we opted for a Takagi–Sugeno fuzzy system, the activation function of our ANFIS' output neuron was linear. In the performance sensitivity study with respect to the nature of the membership functions, we assumed that seven membership functions shared the range of wind speed values from 0 m/s to 25 m/s. ANFIS automatically generates seven fuzzy rules for decision making. Results recorded in Table 6 indicated that Gaussian membership functions yielded the lowest probability density training RMSEs for both Lomé and Cotonou, after 250 iterations.

Table 6. Comparison of membership functions (MF) by their RMSE for Lomé and Cotonou.

Type of MFs	Number of MFs	Number of Iterations	Type of Output	RMSE	
				Lomé	Cotonou
Gaussian	7	250	Linear	4.13×10^{-6}	1.87×10^{-7}
Triangular	7	250	Linear	8.96×10^{-3}	2.60×10^{-2}
Trapezoidal	7	250	Linear	1.73×10^{-2}	3.06×10^{-2}
Sigmoidal	7	250	Linear	1.60×10^{-2}	5.34×10^{-4}

Table 7. Selection of the number of membership functions.

Number of MFs	RMSE	
	Lomé	Cotonou
4	1.3×10^{-3}	1.12×10^{-2}
5	4.70×10^{-3}	1.90×10^{-3}
6	2.02×10^{-2}	8.57×10^{-4}
7	4.13×10^{-6}	1.87×10^{-7}
8	1.71×10^{-5}	6.50×10^{-6}

The performance sensitivity with regard to the number of membership functions is presented in Table 7. For numbers in the range of 4 to 8, the best probability density approximation was found when seven fuzzy rules (membership functions) were used for both sites. In summary, Figure 8 illustrates the type of membership functions and the number of fuzzy rules considered in the design of the ANFIS. Seven Gaussian membership functions characterized our ANFIS design for the sites of Lomé and Cotonou.
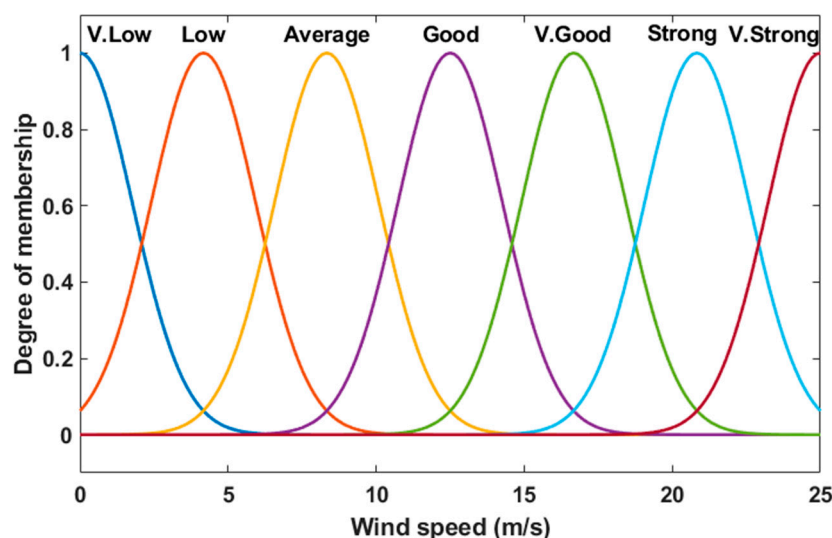
Figure 8. Nature of membership functions and number of fuzzy rules.

4.4.4. SVR Design

Given the non-linear nature of the wind speed distribution fitting problem, we tested three kernel functions: linear, polynomial, and Gaussian. The outcomes of these kernels were compared based on the root mean square error (RMSE) of the output. Results in Table 8 show that the Gaussian kernel outperformed the linear and polynomial kernels. Therefore, the retained support vector regression design used the Gaussian kernel function.

Table 8. Kernel comparison.

Kernels	RMSE	
	Lomé	**Cotonou**
Linear	5.64×10^{-2}	1.34×10^{-1}
Polynomial	4.20×10^{-2}	8.48×10^{-2}
Gaussian	7.04×10^{-4}	3.90×10^{-3}

4.5. Case Study Setup

The purpose of this paper was to compare several methods (EMJ, MLM, MLP, ANFIS and SVR) for evaluating wind energy potential in Togo and Benin. To this end, the case study was structured in the following four steps, for each method j:

- Step 1: use measured data to determine the wind speed probability density function $f_j(v)$;
- Step 2: derive distribution approximation errors e_j from fitting $f_j(v)$ to the empirical histograms for all sites;
- Step 3: compute energy potentials E_j and determine corresponding energy errors ξ_j;
- Step 4: after steps 1–3 are completed for all energy potential assessment methods, compare their statistical performance based on metrics presented in Section 4.3.

5. Results and Discussions

In this section, we first highlight the design parameters obtained for each of the five methods compared in this work. To this end, we present in the next subsection the wind speed characterization results for each method across a range of method-specific parameters. The set of parameters that minimized the histogram adjustment errors was retained for the final design.

5.1. Wind Speed Characterization Performance

It is critical that all probability density functions satisfy the unity area criterion expressed by Equation (36) to be considered as distribution laws. By design, EMJ and MLM naturally satisfy (36). To ensure that the wind speed density functions obtained from the three numerical approaches were distribution laws, we computed the cumulative sums of the probability distribution functions as shown in Table 9 for MLP, ANFIS and SVR.

$$\int_0^{v_{max}} f(v)dv = 1 \tag{36}$$

Table 9. Distribution area.

	MLP	**ANFIS**	**SVR**
Lomé	0.996	0.999	0.995
Cotonou	0.997	0.999	0.996

Because the distribution area was approximately one for all approaches, we could conclude that they were all distribution laws.

Figures 9 and 10 show the wind speed distribution function of each method fitted to the histogram of measured wind speeds on the sites of Lomé and Cotonou.

Performance evaluation metrics described in Section 4 are presented in Table 10 to compare the performance of the five methods. The results showed a better performance of the ANFIS and MLP approaches compared to the other approaches used, regardless of the wind site. From Table 10:

- ANFIS, MLP, and SVR outperformed the two other methods in characterizing the wind speed on both sites;
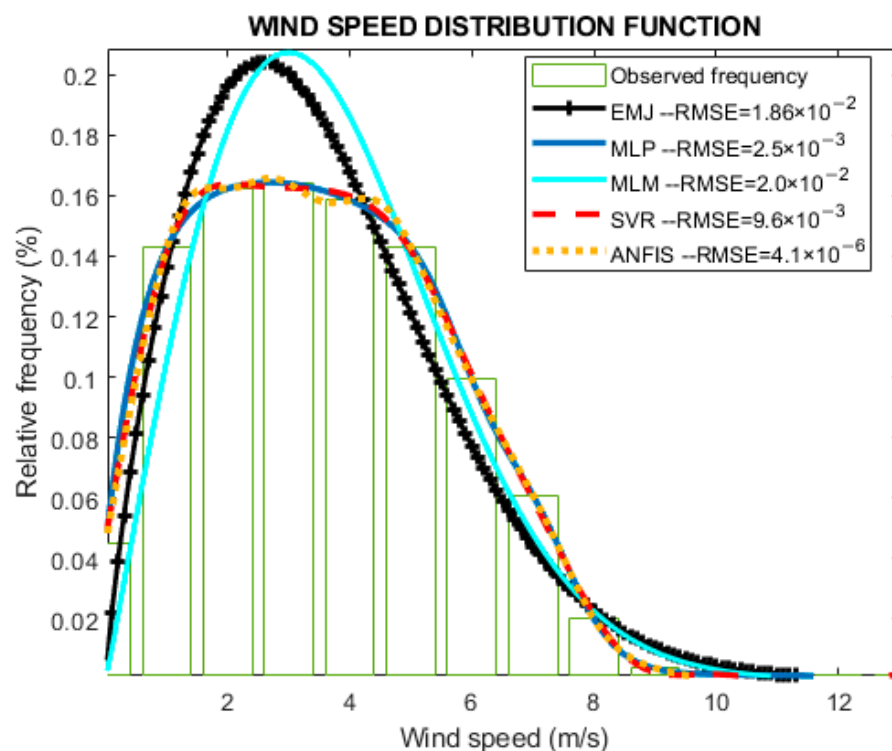- EMJ outperformed MLM on the site of Lomé while MLM outperformed EMJ in Cotonou.

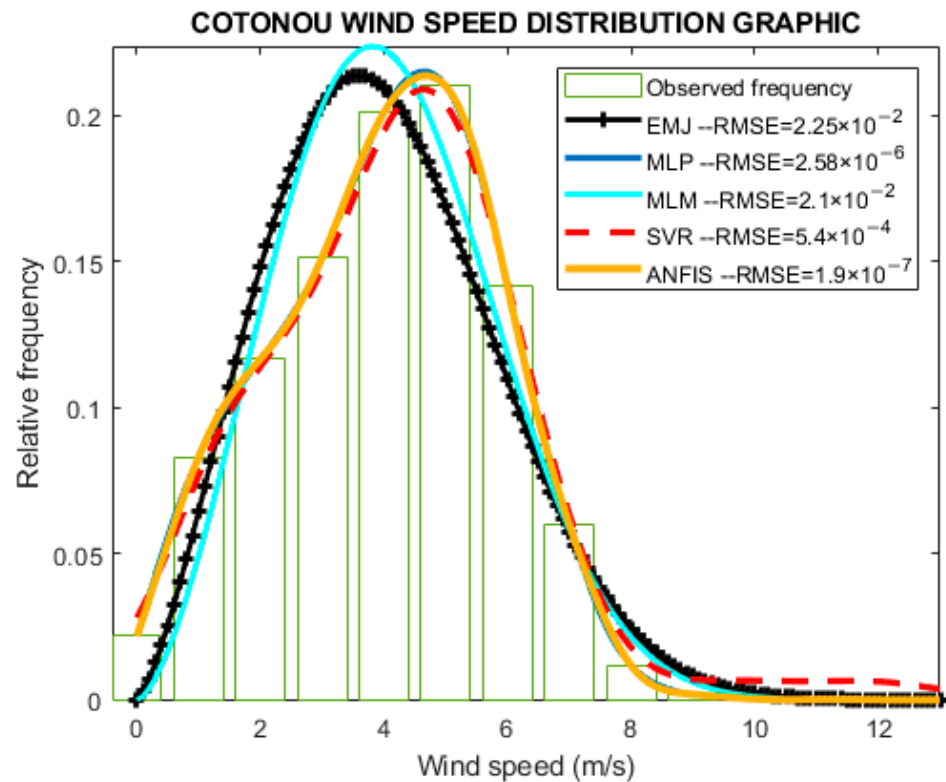**Figure 9.** Wind speed distribution function for the site of Lomé.

Figure 10. Wind speed distribution function for the site of Cotonou.

Table 10. Method comparison.

	EMJ		MLP		MLM		ANFIS		SVR	
	R^2	RMSE	R^2	RMSE	R^2	RMSE	R^2	RMSE	R^2	RMSE
Lomé	0.9687	0.0187	1.000	0.000	0.9649	0.020	1.000	0.000	0.9841	0.009
Cotonou	0.9570	0.0220	1.000	0.000	0.9670	0.021	1.000	0.000	0.9989	0.005

Figures 11 and 12 show that the major challenge EMJ and MLM faced was the prediction of lower wind speed densities. SVR achieved an acceptable performance with significantly low RMSEs.

5.2. Wind Energy Potential Estimation

In this section, we compared the five energy potential assessment methods based on their ability to accurately estimate the available wind energy (E_a in kWh/m^2, see Equation (9)), the recoverable wind energy (E_r in kWh, see Equation (10)) and the wind turbine energy output (E_g in kWh, see Equation (15)). The baseline for this comparison is the raw speed measurement data from which the corresponding energy quantities were computed.
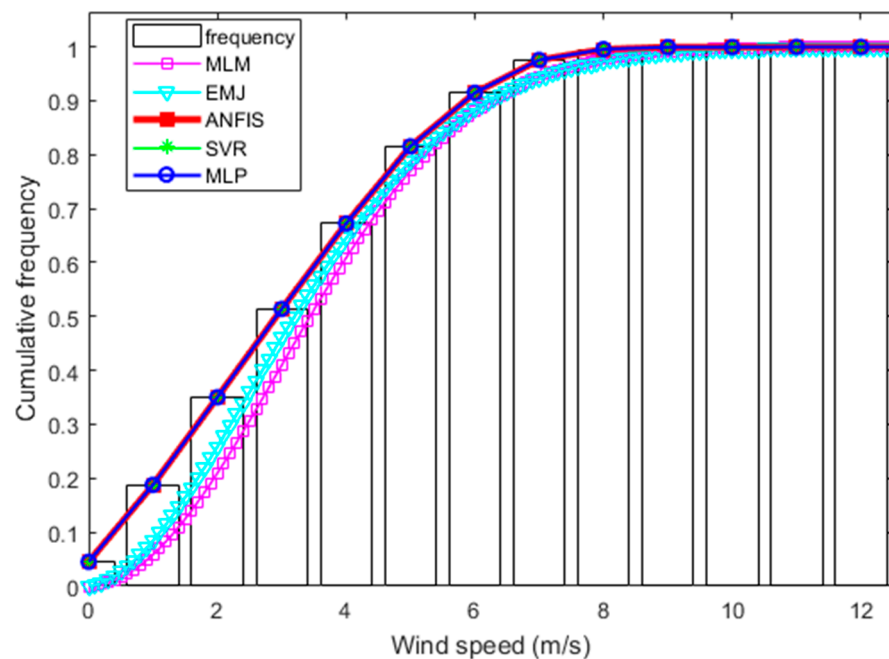
Figure 11. Fitting the cumulative wind speed frequency for the site of Lomé.
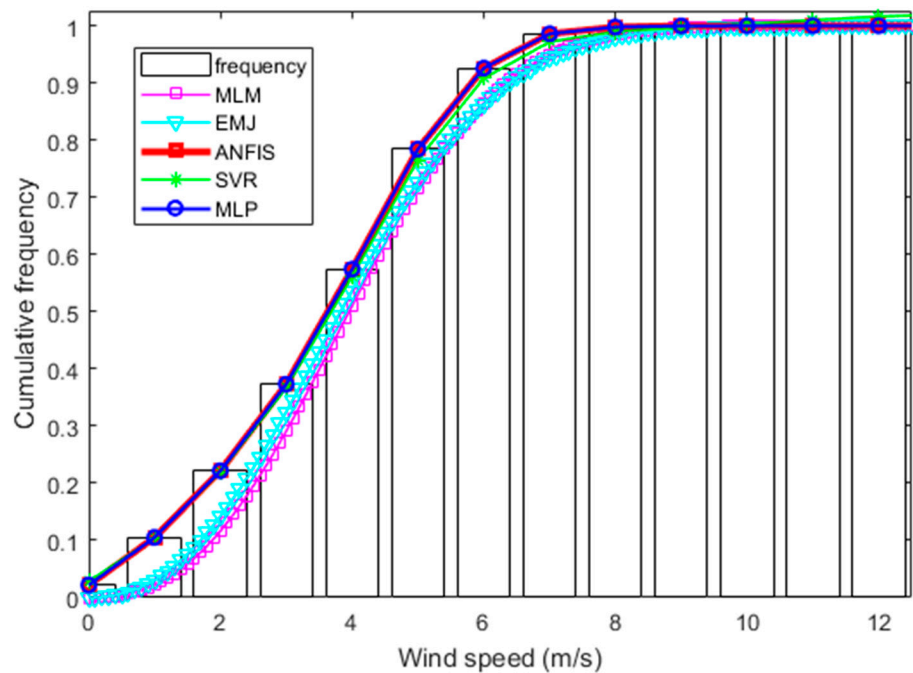

Figure 12. Fitting the cumulative wind speed frequency for the site of Cotonou.

5.2.1. Available Energy Density

For each site, Table 11 shows the observed monthly energy densities as well as the energy densities estimated by MPL, ANFIS, SVR, EMJ, and MLM, respectively. Figures 13 and 14 plot the estimated available energy densities on the y-axis against observed energy densities on the x-axis. A regression line was used to graphically evaluate the performance of each assessment method, while numerically, RMSE was used. ANFIS boasted the least error among all five methods, with an RMSE at least three-orders of magnitude lower. MLM proved to be the second-best method for energy density estimation while SVR was the worst on both sites. In general, SVR overestimated the energy density on the site of Lomé.

Table 11. Available energy density estimation (kWh/m^2).

Month	Lomé						Cotonou					
	Obs.	**MLP**	**ANFIS**	**SVR**	**EMJ**	**MLM**	**Obs.**	**MLP**	**ANFIS**	**SVR**	**EMJ**	**MLM**
Jan.	43.62	43.59	43.62	52.60	44.50	46.59	46.10	46.14	46.10	59.59	45.42	46.16
Feb.	77.54	77.90	77.54	92.71	80.45	82.72	87.52	87.68	87.52	79.94	91.47	90.32
Mar.	87.74	87.87	87.74	121.17	90.42	92.63	96.84	96.23	96.84	89.27	101.89	100.09
Apr.	69.97	69.97	70.04	171.06	72.89	75.42	82.69	82.59	82.69	78.76	85.44	85.56
May	46.96	47.15	46.96	43.74	48.30	50.29	57.68	57.85	57.68	70.34	58.15	59.47
June	57.86	57.35	57.86	66.50	59.75	61.82	71.41	71.33	71.41	89.29	74.04	75.48
July	89.85	89.35	89.85	114.59	91.98	92.42	116.59	116.61	116.59	133.49	120.70	119.51
Aug.	110.61	108.67	110.61	158.28	112.40	112.03	118.36	117.43	118.36	143.79	122.18	121.85
Sep.	92.35	92.28	92.35	110.75	94.20	94.97	100.96	100.35	100.96	116.15	106.59	105.99
Oct.	57.34	57.37	57.34	64.77	58.94	60.81	58.21	57.99	58.20	66.62	59.62	60.64
Nov.	44.90	44.90	44.90	56.86	45.91	47.50	52.70	52.84	52.70	66.44	52.41	52.70
Dec.	39.55	39.63	39.55	52.62	40.12	41.83	47.09	47.04	47.09	61.45	46.21	46.62
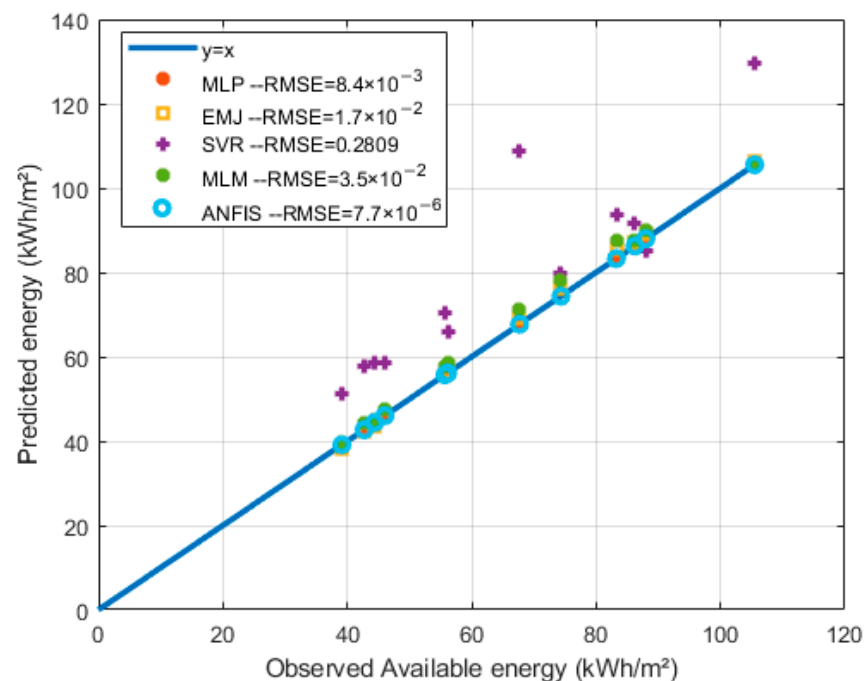
Figure 13. Lomé: Correlation between observed and estimated available energy density.

5.2.2. Recoverable Energy

Table 12 records the monthly recoverable energy E_r in kWh (see Equation (10)) at the sites of Lomé and Cotonou. Observed or actual recoverable energy values were computed from measured wind speed data while estimated recoverable energies were obtained from wind speed probability density estimates given by the five methods presented in Sections 2 and 3. Figures 15 and 16 show the correlation between observed and estimated recoverable energies for the sites of Lomé and Cotonou, respectively.

The results indicated that ANFIS was the best method for estimating the recoverable energy on the sites of Lomé and Cotonou with RMSE values in the order of 10^{-2}. Correlation plots in Figures 15 and 16 show that MLM and EMJ led to the most inaccurate recoverable energy estimates. In fact, for both sites, these methods underestimated the recoverable energy values. This behavior resulted from the overestimation of low-speed densities by the Weibull distribution-based methods, as seen in Figures 5–7. Although SVR yielded acceptable estimates for the site of Lomé, its RMSE on the site of Cotonou was of the same order of magnitude as those of MLM and EMJ. As in the case of energy density estimates, MLP yielded the second most accurate estimates.

Table 12. Recoverable energy estimation (kWh).

| Month	Lomé						Cotonou					
	Obs.	MLP	ANFIS	SVR	EMJ	MLM	Obs.	MLP	ANFIS	SVR	EMJ	MLM
Jan.	1338.96	1487.41	1532.44	1543.50	576.84	911.75	1575.35	1632.74	1733.21	1741.70	675.97	821.84
Feb	2256.12	2400.51	2589.59	2397.26	982.80	1263.56	3028.02	3135.22	3409.51	2259.32	1322.18	1484.56
Mar.	2728.72	2689.27	2817.66	2761.58	1084.95	1373.65	3628.73	3466.82	3754.52	2322.58	1484.77	1679.00
Apr.	2555.64	2271.76	2434.36	2391.24	892.63	1186.90	3149.38	2886.74	3112.28	2281.55	1199.76	1415.63
May	1962.82	1673.98	1774.93	1642.78	607.58	905.78	2288.98	1972.34	2128.36	1861.55	809.24	1007.27
June	2026.72	2045.79	2127.11	2033.82	749.78	1006.57	2508.27	2490.53	2668.06	2392.91	987.93	1272.66
July	2933.38	3059.06	3173.51	3135.84	1225.42	1365.74	3736.94	3904.56	4125.51	3350.62	1701.40	1823.20
Aug.	3496.85	3610.83	3676.50	3655.80	1532.22	1606.99	4325.46	4133.44	4307.88	3930.85	1836.23	1926.84
Sep.	3257.28	3101.21	3118.22	3118.39	1206.89	1345.47	3849.82	3590.79	3762.08	3449.54	1457.29	1782.36
Oct.	2403.33	2087.76	2137.33	2022.03	745.97	967.02	2531.42	2052.42	2220.53	1894.93	838.57	1028.53
Nov.	2001.16	1812.64	1914.96	1920.72	615.12	831.77	2119.30	1919.72	2039.29	1764.69	795.16	919.93
Dec.	1718.32	1614.71	1692.48	1728.40	537.15	806.48	1857.41	1732.89	1842.48	1833.68	701.57	813.13
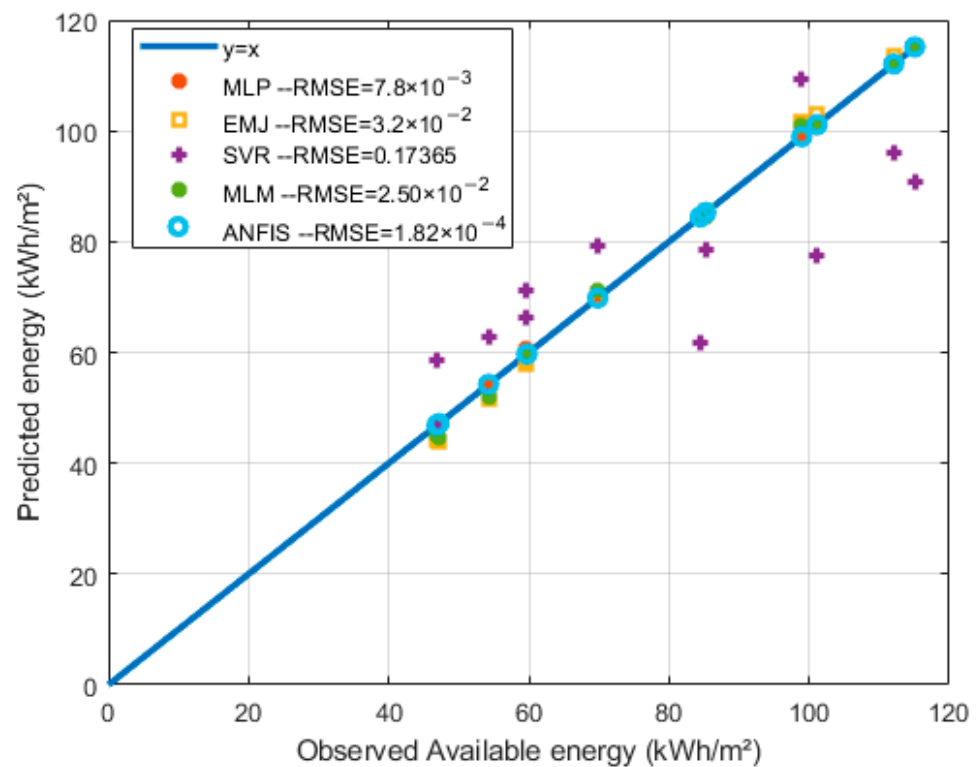
Figure 14. Cotonou: correlation between observed and estimated available energy density.

5.2.3. Wind Turbine Energy Output

Table 13 presents the energy produced or wind turbine energy output E_g in kWh given by Equation (15) on the sites of Lomé and Cotonou. The observed or actual energy output computed from measured wind speed data were compared to the wind turbine energy output estimated using the five methods presented in Sections 2 and 3. Figures 17 and 18 show the correlation between observed and estimated energy output for the sites of Lomé and Cotonou, respectively.
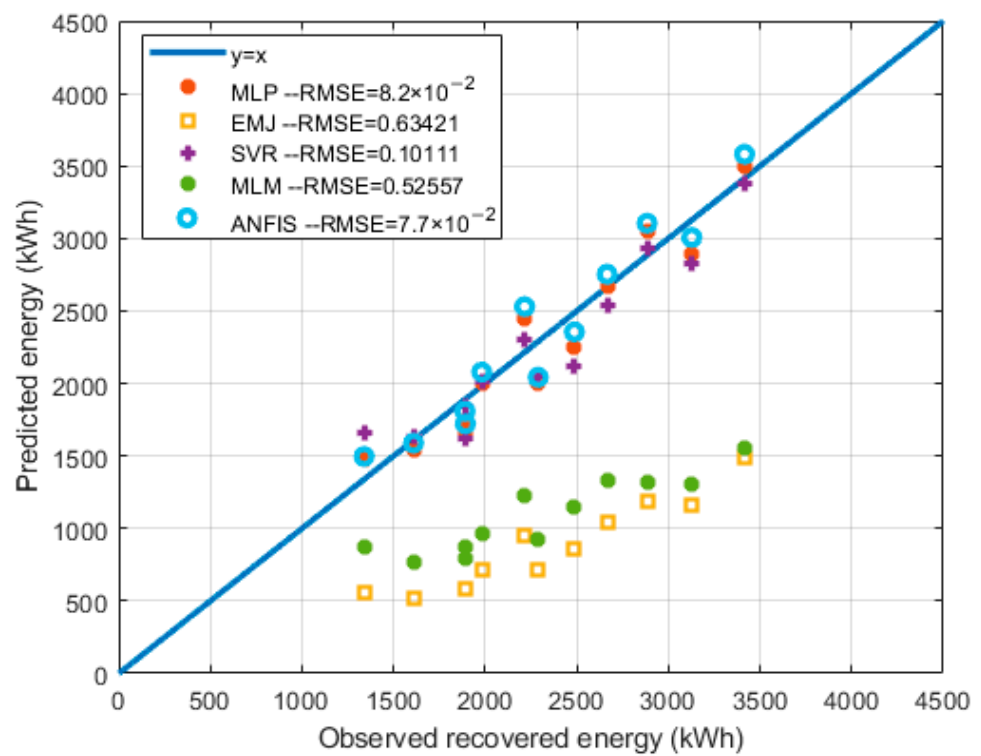
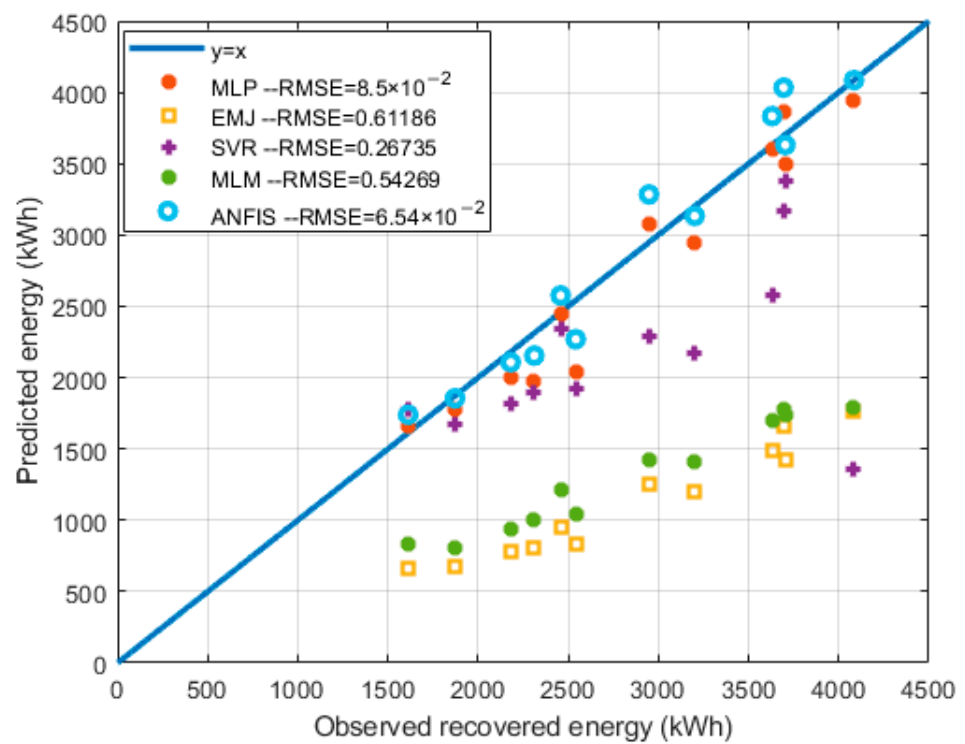**Figure 15.** Correlation between observed and estimated recoverable energy on the site of Lomé.

Figure 16. Cotonou: correlation between observed and estimated recoverable energy.

Table 13. Wind turbine output energy estimation (kWh).

Month	Lomé						Cotonou					
	Obs	**MLP**	**ANFIS**	**SVR**	**EMJ**	**MLM**	**Obs**	**MLP**	**ANFIS**	**SVR**	**EMJ**	**MLM**
Jan.	44,819.60	44,805.30	44,819.57	54,004.19	40,591.66	45,473.75	47,268.98	47,317.13	47,268.95	61,302.58	45,494.08	46,781.36
Feb.	80,666.95	80,371.97	80,666.90	89,951.98	79,225.91	83,570.95	92,295.19	92,479.42	92,295.22	80,897.66	95,352.61	94,657.03
Mar.	91,143.12	91,333.28	91,143.00	115,021.50	88,836.31	93,463.65	102,517.44	101,898.57	102,517.48	90,686.23	106,856.16	105,490.33
Apr.	72,372.36	72,281.81	72,339.55	112,155.15	71,901.73	76,209.15	86,458.74	86,376.54	86,458.75	78,097.55	88,347.20	89,214.99
May	48,072.94	47,625.44	48,073.04	42,527.44	47,417.46	50,712.13	58,957.99	58,815.27	58,958.16	60,432.51	59,142.45	61,048.44
June	59,907.14	59,463.21	59,907.13	63,890.18	58,877.55	62,420.96	74,447.50	74,353.51	74,447.54	85,634.60	74,949.03	77,799.98
July	94,292.97	93,343.02	94,293.18	114,702.58	94,203.07	95,524.21	122,945.80	123,028.00	122,946.01	135,774.10	126,909.05	126,143.37
Aug.	115,991.63	114,254.39	115,991.31	152,781.04	116,972.61	116,997.09	125,951.93	124,789.52	125,951.77	152,155.07	130,072.52	129,943.30
Sep.	98,024.08	98,078.04	98,023.85	116,612.05	93,053.45	95,641.97	108,463.80	107,869.25	108,463.75	124,577.80	105,378.70	109,467.25
Oct.	60,993.18	61,047.57	60,993.09	67,561.40	57,185.18	61,151.65	60,397.15	60,154.68	60,404.49	60,736.78	60,828.04	62,378.37
Nov.	50,490.76	50,490.78	50,490.74	62,900.26	47,248.99	50,637.15	54,363.16	54,502.78	54,363.20	58,051.67	53,762.00	54,173.96
Dec.	44,669.80	44,758.06	44,669.77	58,326.92	41,867.41	45,427.11	48,226.40	48,168.58	48,226.40	57,147.80	47,100.35	47,592.87

Correlation study results showed that the Weibull distribution-based methods MLM and EMJ consistently underestimated the wind turbine energy output. Although SVR achieved acceptable estimates on the site of Lomé, it mostly underestimated the wind energy output values on the site of Cotonou. ANFIS and MLP proved to be the most accurate on both sites as shown by Figures 17 and 18.
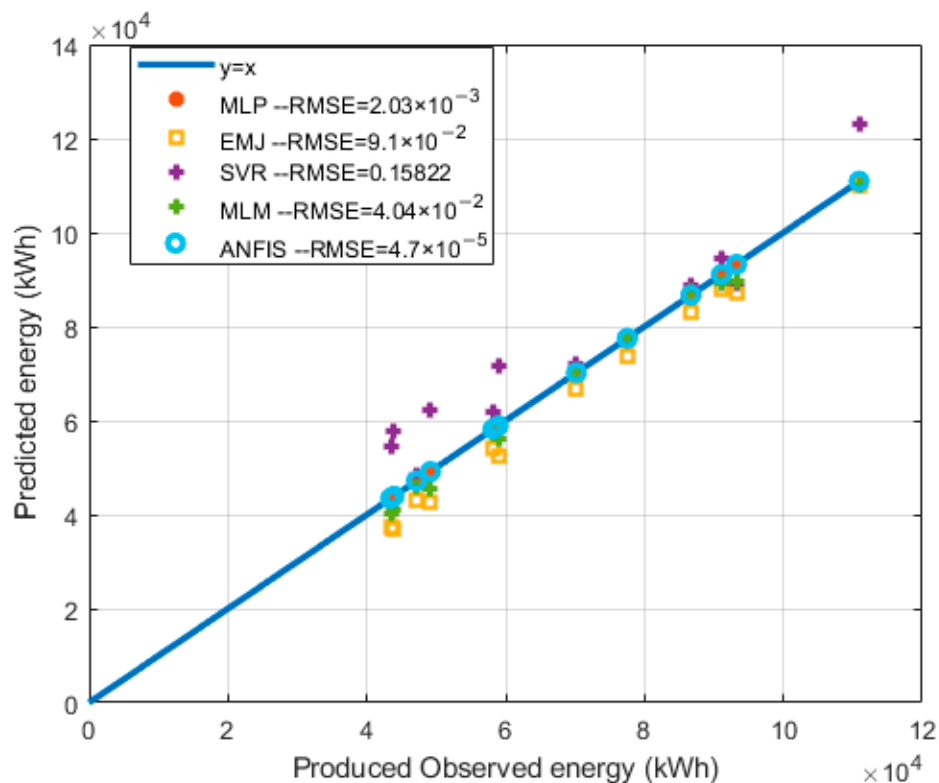

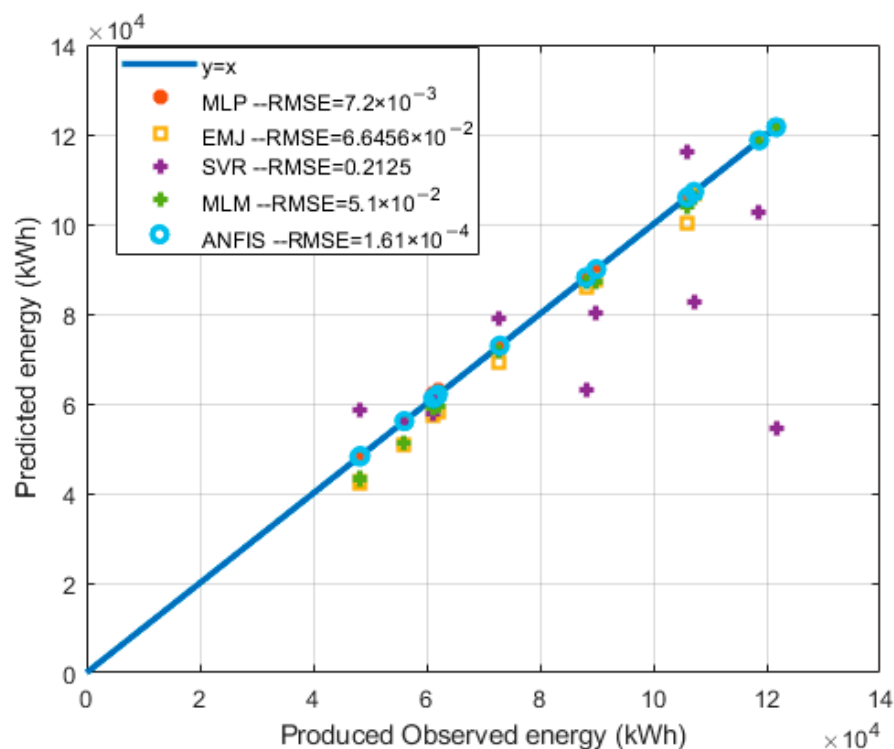**Figure 17.** Lomé: correlation between observed and estimated wind energy output.

Figure 18. Cotonou: correlation between observed and estimated wind energy output.

6. Conclusions

To investigate which wind energy resource estimation model is best for the sites of Benin and Togo, this paper reviewed and compared five wind energy potential evaluation methods, namely: the ANFIS, the MLP, the SVR, the EMJ, and the MLM. The case study results validated that an accurate estimation of the speed distribution law has a significant impact on the accuracy of wind energy potential estimation. A performance comparison of the aforementioned methods with regard to available energy, recoverable energy and turbine output energy, established that the ANFIS approach offered the most accurate estimation on both sites. Following the ANFIS was the MLP method. These two neural network-based methods clearly outperformed the three other methods investigated in this work In fact, the orders of magnitude of the root mean squared error in estimating the recoverable energy using ANFIS were, respectively, 10^{-4} and 10^{-5} for Lomé and Cotonou, while MLP achieved an RMSE order of magnitude of 10^{-3} for both sites. Despite being commonly used in wind energy potential estimation projects, the Weibull distribution-based methods EMJ and MLM proved the least accurate, especially in estimating recoverable energy and wind turbine energy output on both sites. Even though SVR ranks as the third best method, it was unstable across estimation types and wind sites. Its performance was not consistent for both sites and was less recommendable for the site of Cotonou. Therefore, the top two wind energy potential estimation methods recommendable for the sites of Lomé (Togo) and Cotonou (Benin) were the Takagi–Sugeno fuzzy system-based ANFIS with Gaussian membership function controlled by seven fuzzy rules, and the MLP with nine neurons in the hidden layer.

Author Contributions: Conceptualization, A.A.S., K.S.A.S. and P.A.A.; methodology, A.A.S., K.S.A.S. and M.K.K.; software, P.A.A.; validation, A.A.S., K.S.A.S. and M.K.K.; formal analysis, M.K.K. and A.A.S.; investigation, K.S.A.S.; resources, K.S.A.S. and A.A.S.; data curation, A.A.S. and P.A.A.; writing—original draft preparation, P.A.A. and K.S.A.S.; writing—review and editing, K.S.A.S.; visualization, P.A.A.; supervision, A.A.S., K.S.A.S. and M.K.K.; project administration, A.A.S. and K.S.A.S.; funding acquisition, A.A.S. and K.S.A.S. All authors have read and agreed to the published version of the manuscript.

Institutional Review Board Statement: Not applicable.

Informed Consent Statement: Not applicable.

Data Availability Statement: Restrictions apply to the availability of data. Contact authors for required permissions.

Conflicts of Interest: The authors declare no conflict of interest.

Abbreviations

ρ	air density
S	area swept by the blades of the wind turbine
E_a	available energy
P_m	available wind power
F	cumulative density function
E_g	generated energy
v	instantaneous wind speed
V_c	maximum or cut-out speed of the wind turbine.
Φ	nonlinear transformation function
c	scale factor
k	shape or form factor
σ	standard deviation
V_r	rated speed of the wind turbine
E_r	recovery energy
V_s	starting or cut-in speed of the wind turbine;
v	wind speed
f	wind speed distribution function
ANFIS	adaptative neuro-fuzzy inference system
ANN	artificial neuron network
CPU	central processing unit
R^2	coefficient of determination
EMJ	empirical method of Justus
EML	empirical method of Lysen
EPFM	energy pattern factor method
GFNN	generalized feed-forward neural network
GM	graphical method
MLM	maximum likelihood method
MMLM	modified maximum likelihood method
MLP	multilayer perceptron
RBF	radial basic function
RMSE	root mean squared error
SVM	support vector machine
SVR	support vector regression

References

1. Energy Information Administration; Office of Integrated Analysis and Forecasting; U.S. Department of Energy. Report #DOE/EIA-0484(2003). November 2003, Washington, DC 20585, May 2003. Available online: www.eia.doe.gov/oiaf/ieo/download.html (accessed on 15 August 2021).

2. World Data. Energy Consumption in Benin. 2019. Available online: https://www.worlddata.info/africa/benin/energy-consumption.php (accessed on 10 August 2021).
3. World Data. Energy Consumption in Togo. 2019. Available online: https://www.worlddata.info/africa/togo/energy-consumption.php (accessed on 10 August 2021).
4. World Data. Energy Consumption in the United States of America. 2019. Available online: https://www.worlddata.info/america/usa/energy-consumption.php (accessed on 13 August 2021).
5. International Renewable Energy Agency. *Planning and Prospects for Renewable Power: West Africa. 2018 Report*; International Renewable Energy Agency: Abu Dhabi, United Arab Emirates, 2018.
6. USAID Power Africa. Benin Power Africa Fact Sheet. 2019. Available online: https://www.usaid.gov/powerafrica/benin (accessed on 13 August 2021).
7. USAID Power Africa. Togo Power Africa Fact Sheet. 2019. Available online: https://www.usaid.gov/powerafrica/togo (accessed on 17 August 2021).
8. Haque, A.U.; Mandal, P.; Kaye, M.E.; Meng, J.; Chang, L.; Senjyu, T. A new strategy for predicting short-term wind speed using soft computing models. *Renew. Sustain. Energy Rev.* **2012**, *16*, 4563–4573. [CrossRef]
9. Petković, D.; Pavlović, N.T.; Ćojbašić, Ž. Wind farm efficiency by adaptive neuro-fuzzy strategy. *Int. J. Electr. Power Energy Syst.* **2016**, *81*, 215–221. [CrossRef]
10. Zhao, H.; Wu, Q.; Hu, S.; Xu, H.; Rasmussen, C.N. Review of energy storage system for wind power integration support. *Appl. Energy* **2015**, *137*, 545–553. [CrossRef]
11. Weigt, H. Germany's wind energy: The potential for fossil capacity replacement and cost saving. *Appl. Energy* **2009**, *86*, 1857–1863. [CrossRef]
12. Snyder, B.; Kaiser, M.J. A comparison of offshore wind power development in europe and the U.S.: Patterns and drivers of development. *Appl. Energy* **2009**, *86*, 1845–1856. [CrossRef]
13. Radics, K.; Bartholy, J. Estimating and modelling the wind resource of Hungary. *Renew. Sustain. Energy Rev.* **2008**, *12*, 874–882. [CrossRef]
14. Davidson, M.; Zhang, D.; Xiong, W.; Zhang, X.; Karplus, V.J. Modelling the potential for wind energy integration on China's coal-heavy electricity grid. *Nat. Energy* **2016**, *1*, 16086. [CrossRef]
15. Shata, A.A.; Hanitsch, R. Evaluation of wind energy potential and electricity generation on the coast of Mediterranean Sea in Egypt. *Renew. Energy* **2006**, *31*, 1183–1202. [CrossRef]
16. Et, L.T.; Sow, G.; Fall, S.S.; Kasse, M.; Sylla, E.; Thioye, S. A Neural network approach for wind ressource and wind generators production. *Appl. Energy* **2010**, *87*, 1744–1748.
17. Li, G.; Shi, J. Application of Bayesian model averaging in modeling long-term wind speed distributions. *Renew. Energy* **2010**, *35*, 1192–1202. [CrossRef]
18. Morgan, E.C.; Lackner, M.; Vogel, R.M.; Baise, L.G. Probability distributions for offshore wind speeds. *Energy Convers. Manag.* **2011**, *52*, 15–26. [CrossRef]
19. Carta, J.A.; Ramírez, P.; Velázquez, S. Influence of the level of fit of a density probability function to wind-speed data on the WECS mean power output estimation. *Energy Convers. Manag.* **2008**, *49*, 2647–2655. [CrossRef]
20. Akdağ, S.A.; Dinler, A. A new method to estimate Weibull parameters for wind energy applications. *Energy Convers. Manag.* **2009**, *50*, 1761–1766. [CrossRef]
21. Safari, B. Modeling wind speed and wind power distributions in Rwanda. *Renew. Sustain. Energy Rev.* **2011**, *15*, 925–935. [CrossRef]
22. Masseran, N.; Razali, A.M.; Ibrahim, K.; Zaharim, A.; Sopian, K. The Probability Distribution Model of Wind Speed over East Malaysia. *Res. J. Appl. Sci. Eng. Technol.* **2013**, *6*, 1774–1779. [CrossRef]
23. Chang, T.P. Performance comparison of six numerical methods in estimating Weibull parameters for wind energy application. *Appl. Energy* **2011**, *88*, 272–282. [CrossRef]
24. Saleh, H.; El-Azm Aly, A.A.; Abdel-Hady, S. Assessment of different methods used to estimate Weibull distribution parameters for wind speed in Zafarana wind farm, Suez Gulf, Egypt. *Energy* **2012**, *44*, 710–719. [CrossRef]
25. Ettoumi, Y.F.; Sauvageot, H.; Adane, A.-E.-H. Statistical bivariate modelling of wind using first-order Markov chain and Weibull distribution. *Renew. Energy* **2003**, *28*, 1787–1802. [CrossRef]
26. Shu, Z.; Li, Q.; Chan, P.W. Investigation of offshore wind energy potential in Hong Kong based on Weibull distribution function. *Appl. Energy* **2015**, *156*, 362–373. [CrossRef]
27. Celik, A. Weibull representative compressed wind speed data for energy and performance calculations of wind energy systems. *Energy Convers. Manag.* **2003**, *44*, 3057–3072. [CrossRef]
28. Ben Amar, F.; Elamouri, M.; Dhifaoui, R. Energy assessment of the first wind farm section of Sidi Daoud, Tunisia. *Renew. Energy* **2008**, *33*, 2311–2321. [CrossRef]
29. Mathew, S.; Pandey, K.; Kumar, V.A. Analysis of wind regimes for energy estimation. *Renew. Energy* **2002**, *25*, 381–399. [CrossRef]
30. Murthy, K.S.R.; Rahi, O.P. Wind Power Density Estimation Using Rayleigh Probability Distribution Function. In *Applications of Artificial Intelligence Techniques in Engineering*; Springer: Berlin/Heidelberg, Germany, 2019; pp. 265–275.
31. Ahmed, A.S. Wind energy characteristics and wind park installation in Shark El-Ouinat, Egypt. *Renew. Sustain. Energy Rev.* **2018**, *82*, 734–742. [CrossRef]

32. Mazzeo, D.; Oliveti, G.; Labonia, E. Estimation of wind speed probability density function using a mixture of two truncated normal distributions. *Renew. Energy* **2018**, *115*, 1260–1280. [CrossRef]

33. Samal, R.K.; Tripathy, M. Estimating wind speed probability distribution based on measured data at Burla in Odisha, India. *Energy Sources, Part A: Recover. Util. Environ. Eff.* **2018**, *41*, 918–930. [CrossRef]

34. Salami, A.A.; Ajavon, A.S.A.; Kodjo, K.M.; Ouedraogo, S.; Bédja, K.-S. The Use of Odd and Even Class Wind Speed Time Series of Distribution Histogram to Estimate Weibull Parameters. *Int. J. Renew. Energy Dev.* **2018**, *7*, 139–150. [CrossRef]

35. Stevens, M.J.M.; Smulders, P.T. The estimation of the parameters of the Weibull wind speed distribution for wind energy utilization purposes. *Wind. Eng.* **1979**, *3*, 132–145.

36. Azad, A.K.; Rasul, M.G.; Alam, M.M.; Uddin, S.A.; Mondal, S.K. Analysis of wind energy conversion system using Weibull distribution. *Procedia Eng.* **2014**, *90*, 725–732. [CrossRef]

37. Elamouri, M.; Ben Amar, F. Wind energy potential in Tunisia. *Renew. Energy* **2008**, *33*, 758–768. [CrossRef]

38. Kiss, P.; Jánosi, I.M. Comprehensive empirical analysis of ERA-40 surface wind speed distribution over Europe. *Energy Convers. Manag.* **2008**, *49*, 2142–2151. [CrossRef]

39. Celik, A.N. A statistical analysis of wind power density based on the Weibull and Rayleigh models at the southern region of Turkey. *Renew. Energy* **2004**, *29*, 593–604. [CrossRef]

40. Safari, B.; Gasore, J. A statistical investigation of wind characteristics and wind energy potential based on the Weibull and Rayleigh models in Rwanda. *Renew. Energy* **2010**, *35*, 2874–2880. [CrossRef]

41. Shu, Z.; Li, Q.; Chan, P.W. Statistical analysis of wind characteristics and wind energy potential in Hong Kong. *Energy Convers. Manag.* **2015**, *101*, 644–657. [CrossRef]

42. Ucar, A.; Balo, F. Investigation of wind characteristics and assessment of wind generation potentiality in Uludag-Bursa, Turkey. *Appl. Energy* **2009**, *86*, 333–339. [CrossRef]

43. Chang, T.-J.; Wu, Y.-T.; Hsu, H.-Y.; Chu, C.-R.; Liao, C.-M. Assessment of wind characteristics and wind turbine characteristics in Taiwan. *Renew. Energy* **2003**, *28*, 851–871. [CrossRef]

44. Salami, A.A.; Ajavon, A.S.A.; Kodjo, M.K.; Bedja, K.-S. Contribution to improving the modeling of wind and evaluation of the wind potential of the site of Lome: Problems of taking into account the frequency of calm winds. *Renew. Energy* **2013**, *50*, 449–455. [CrossRef]

45. Shamshirband, S.; Mohammadi, K.; Tong, C.W.; Petković, D.; Porcu, E.; Mostafaeipour, A.; Ch, S.; Sedaghat, A. Application of extreme learning machine for estimation of wind speed distribution. *Clim. Dyn.* **2016**, *46*, 1893–1907. [CrossRef]

46. Rocha PA, C.; de Sousa, R.C.; de Andrade, C.F.; da Silva, M.E.V. Comparison of seven numerical methods for determining Weibull parameters for wind energy generation in the northeast region of Brazil. *Appl. Energy* **2012**, *89*, 395–400. [CrossRef]

47. Justus, C.G.; Hargraves, W.R.; Mikhail, A.; Graber, D. Methods for Estimating Wind Speed Frequency Distributions. *J. Appl. Meteorol.* **1978**, *17*, 350–353. [CrossRef]

48. Weisser, D. A wind energy analysis of Grenada: An estimation using the 'Weibull' density function. *Renew. Energy* **2003**, *28*, 1803–1812. [CrossRef]

49. Asghar, A.B.; Liu, X. Estimation of wind speed probability distribution and wind energy potential using adaptive neuro-fuzzy methodology. *Neurocomputing* **2018**, *287*, 58–67. [CrossRef]

50. Tizgui, I.; El Guezar, F.; Bouzahir, H.; Benaid, B. Comparison of methods in estimating Weibull parameters for wind energy applications. *Int. J. Energy Sect. Manag.* **2017**, *11*, 650–663. [CrossRef]

51. Mabel, M.C.; Fernandez, E. Estimation of Energy Yield From Wind Farms Using Artificial Neural Networks. *IEEE Trans. Energy Convers.* **2009**, *24*, 459–464. [CrossRef]

52. Celik, A.N.; Kolhe, M. Generalized feed-forward based method for wind energy prediction. *Appl. Energy* **2013**, *101*, 582–588. [CrossRef]

53. Mohandes, M.; Rehman, S.; Rahman, S. Estimation of wind speed profile using adaptive neuro-fuzzy inference system (ANFIS). *Appl. Energy* **2011**, *88*, 4024–4032. [CrossRef]

54. Seguro, J.; Lambert, T. Modern estimation of the parameters of the Weibull wind speed distribution for wind energy analysis. *J. Wind Eng. Ind. Aerodyn.* **2000**, *85*, 75–84. [CrossRef]

55. Singh, S.; Bhatti, T.S.; Kothari, D.P. Wind Power Estimation Using Artificial Neural Network. *J. Energy Eng.* **2007**, *133*, 46–52. [CrossRef]

56. Fadare, D. The application of artificial neural networks to mapping of wind speed profile for energy application in Nigeria. *Appl. Energy* **2010**, *87*, 934–942. [CrossRef]

57. Arslan, O. Erratum to "Technoeconomic analysis of electricity generation from wind energy in Kutahya, Turkey" [Energy (2010) 35: 120–131]. *Energy* **2010**, *35*, 1865. [CrossRef]

58. Malik, A.; Al-Badi, A.H. Economics of wind turbine as an energy fuel saver e a case study for remote application in Oman. *Energy* **2009**, *34*, 1573–1578. [CrossRef]

59. Liu, F.J.; Chang, T.P. Validity analysis of maximum entropy distribution based on different moment constraints for wind energy assessment. *Energy* **2011**, *36*, 1820–1826. [CrossRef]

60. Chang, T.-P.; Liu, F.-J.; Ko, H.-H.; Cheng, S.-P.; Sun, L.-C.; Kuo, S.-C. Comparative analysis on power curve models of wind turbine generator in estimating capacity factor. *Energy* **2014**, *73*, 88–95. [CrossRef]

61. Merzouk, N.K. Evaluation du Gisement Energétique Eolien Contribution à la Détermination du Profil Vertical de la Vitesse du vent en Algérie. Ph.D. Thesis, Université Abou Bekr Belkaid De Tlemcen, Tlemcen, Algeria, 2016.

62. Manwell, J.F.; McGowan, J.G.; Rogers, A.L. *Book Review: Wind Energy Explained: Theory, Design and Application*; John Wiley & Sons: Chichester, UK, 2006; Volume 30, pp. 169–170. [CrossRef]

63. Wais, P. Two and three-parameter Weibull distribution in available wind power analysis. *Renew. Energy* **2017**, *103*, 15–29. [CrossRef]

64. Qing, X. Statistical analysis of wind energy characteristics in Santiago island, Cape Verde. *Renew. Energy* **2018**, *115*, 448–461. [CrossRef]

65. Artin, E. *The Gamma Function*; Courier Dover Publications: Mineola, NY, USA, 2015.

66. Casella, G.; Berger, R.L. *Statistical Inference*; Duxbury: Pacific Grove, CA, USA, 2002; Volume 2.

67. Kidmo, D.K.; Danwe, R.; Doka, S.Y.; Djongyang, N. Statistical analysis of wind speed distribution based on six Weibull Methods for wind power evaluation in Garoua, Cameroon. *Rev. Energ. Renouvelables* **2015**, *18*, 105–125.

68. Liu, F.; Sun, F.; Liu, W.; Wang, T.; Wang, H.; Wang, X.; Lim, W.H. On wind speed pattern and energy potential in China. *Appl. Energy* **2018**, *236*, 867–876. [CrossRef]

69. Loukatou, A.; Howell, S.; Johnson, P.; Duck, P. Stochastic wind speed modelling for estimation of expected wind power output. *Appl. Energy* **2018**, *228*, 1328–1340. [CrossRef]

70. Kantar, Y.M.; Usta, I. Analysis of wind speed distributions: Wind distribution function derived from minimum cross entropy principles as better alternative to Weibull function. *Energy Convers. Manag.* **2008**, *49*, 962–973. [CrossRef]

71. Seo, S.; Oh, S.-D.; Kwak, H.-Y. Wind turbine power curve modeling using maximum likelihood estimation method. *Renew. Energy* **2018**, *136*, 1164–1169. [CrossRef]

72. Asefa, T.; Kemblowski, M.; McKee, M.; Khalil, A. Multi-time scale stream flow predictions: The support vector machines approach. *J. Hydrol.* **2006**, *318*, 7–16. [CrossRef]

73. Kalogirou, S.A. Applications of artificial neural-networks for energy systems. *Appl. Energy* **2000**, *67*, 17–35. [CrossRef]

74. Cybenko, G. Approximation by superpositions of a sigmoidal function. *Math. Control. Signals Syst.* **1989**, *2*, 303–314. [CrossRef]

75. Hornik, K.; Stinchcombe, M.; White, H. Multilayer feedforward networks are universal approximators. *Neural Netw.* **1989**, *2*, 359–366. [CrossRef]

76. Li, S.; O'Hair, E.; Giesselmann, M. Using neural networks to predict wind power generation. In Proceedings of the 1997 International Solar Energy Conferenc, Washington, DC, USA, 27–30 April 1997; pp. 415–420.

77. Li, S.; Wunsch, D.C.; O'Hair, E.; Giesselmann, M.G. Comparative Analysis of Regression and Artificial Neural Network Models for Wind Turbine Power Curve Estimation. *J. Sol. Energy Eng.* **2001**, *123*, 327–332. [CrossRef]

78. Cabodevila, G. *Commande et Identification Floue*; École Nationale Supérieure de Mécanique et des Microtechniques: Besançon, France, 2005.

79. Touzet, C.; Giambiasi, N. Application of connectionist models to fuzzy inference systems. In *Parallelization in Inference Systems. Lecture Notes in Computer Science*; Fronhöfer, B., Wrightson, G., Eds.; Springer: Berlin/Heidelberg, Germany, 1992; Volume 590. [CrossRef]

80. Vapnik, V.N. The Nature of Statistical Learning Theory. *Technometrics* **1997**, *38*, 409.

81. Hellmann, G. *Über die Bewegung der Luft in den Untersten Schichten der Atmosphäre*; Kgl. Akademie der Wissenschaften [G.] Reimer: Berlin, Germany, 1914.

82. Lackner, M.A.; Rogers, A.L.; Manwell, J.F.; McGowan, J.G. A new method for improved hub height mean wind speed estimates using short-term hub height data. *Renew. Energy* **2010**, *35*, 2340–2347. [CrossRef]

83. Hellman, G. Uber die Bewegung der Luft in den untersten Schichten der atmosphere. *Meteorol Z* **1916**, *34*, 273.

84. Tchinda, R.; Kendjio, J.; Kaptouom, E.; Njomo, D. Estimation of mean wind energy available in far north Cameroon. *Energy Convers. Manag.* **2000**, *41*, 1917–1929. [CrossRef]

85. Counihan, J. Adiabatic atmospheric boundary layers: A review and analysis of data from the period 1880–1972. *Atmos. Environ. (1967)* **1975**, *9*, 871–905. [CrossRef]

86. Justus, C.G. *Winds and Wind System Performance*; Research supported by the National Science Foundation and Energy Research and Development Administration; Franklin Institute Press: Philadelphia, PA, USA, 1978; Volume 120, p. 1978.

87. Irwin, J.S. A theoretical variation of the wind profile power-law exponent as a function of surface roughness and stability. *Atmos. Environ. (1967)* **1979**, *13*, 191–194. [CrossRef]

88. Spera David, A. (Ed.) *Wind Turbine Technology: Fundamental Concepts of Wind Turbine Engineering*; ASME Press: New York, NY, USA, 1994; Volume 3.

89. Van den Berg, G.P. Wind turbine power and sound in relation to atmospheric stability. *Wind. Energy Int. J. Prog. Appl. Wind. Power Convers. Technol.* **2008**, *11*, 151–169. [CrossRef]

90. Farrugia, R.N. The wind shear exponent in a Mediterranean island climate. *Renew. Energy* **2003**, *28*, 647–653. [CrossRef]

91. Rehman, S.; Al-Abbadi, N.M. Wind shear coefficient, turbulence intensity and wind power potential assessment for Dhulom, Saudi Arabia. *Renew. Energy* **2008**, *33*, 2653–2660. [CrossRef]

92. Poje, D.; Cividini, B. Assessment of wind energy potential in croatia. *Sol. Energy* **1988**, *41*, 543–554. [CrossRef]

93. Mudasser, M.; Yiridoe, E.K.; Corscadden, K. Economic feasibility of large community feed-in tariff-eligible wind energy production in Nova Scotia. *Energy Policy* **2013**, *62*, 966–977. [CrossRef]

94. Kapluhan, E. Rüzgar enerjisi uygulamalarina bir örnek: Sincik (adiyaman) rüzgar enerji santrali. *J. Int. Soc. Res. June* **2017**, *10*, 305–322. [CrossRef]
95. Salami, A.A.; Ajavon, A.S.A.; Kodjo, M.K.; Bedja, K. Evaluation of wind potential for an optimal choice of wind turbine generator on the sites of Lomé, Accra, and Cotonou located in the Gulf of Guinea. *Int. J. Renew. Energy Dev.* **2016**, *5*, 211–223. [CrossRef]
96. ENERCON. E-44. 2022. Available online: https://www.enercon.de/fr/produits/ep-1/e-44/ (accessed on 13 August 2021).
97. ENERCON. E-48. 2022. Available online: https://www.enercon.de/fr/produits/ep-1/e-48/ (accessed on 13 August 2021).
98. ENERCON. E-53. 2022. Available online: https://www.enercon.de/fr/produits/ep-1/e-53/ (accessed on 15 August 2021).
99. Mohammadi, K.; Shamshirband, S.; Yee, P.L.; Petković, D.; Zamani, M.; Ch, S. Predicting the wind power density based upon extreme learning machine. *Energy* **2015**, *86*, 232–239. [CrossRef]